



# Corrosion inhibition of magnesium alloy AZ31 in chloride-containing solutions by aqueous permanganate

Maria A. Osipenko<sup>1</sup> · Aliaksandr A. Kasach<sup>2</sup> · Janusz Adamiec<sup>3</sup> · Małgorzata Zimowska<sup>4</sup> · Irina I. Kurilo<sup>1</sup> · Dzmitry S. Kharytonau<sup>4</sup>

Received: 14 December 2022 / Revised: 9 February 2023 / Accepted: 13 March 2023 / Published online: 4 April 2023  
© The Author(s) 2023

## Abstract

In this work, corrosion of the AZ31 magnesium alloy was examined in 0.05 M NaCl solutions containing 0.01–0.150 mol/dm<sup>3</sup> of potassium permanganate as a corrosion inhibitor. A set of electrochemical impedance spectroscopy, linear sweep voltammetry, and hydrogen evolution measurements revealed high inhibitor effectiveness at relatively high (0.150 mol/dm<sup>3</sup>) KMnO<sub>4</sub> concentrations. Based on data of energy-dispersive X-ray analysis, scanning electron microscopy, and Raman spectroscopy, a mechanism of the corrosion inhibition of AZ31 alloy by potassium permanganate in chloride-containing media was proposed.

**Keywords** Magnesium alloy · EIS · Corrosion · Corrosion inhibitor · Corrosion mechanism

## Introduction

Magnesium and its alloys are characterized by low density (1.74–1.95 g/cm<sup>3</sup>), high strength-to-weight ratio, non-toxicity, biocompatibility, and good machinability. Due to these properties, magnesium and its alloys are widely used in automotive, aircraft, aerospace technology, and medicine [1]. Magnesium belongs to active metals ( $E_{\text{Mg}^{2+}/\text{Mg}^0}^0 = -2.38$  V), and it actively corrodes in aqueous solutions, with the formation of a surface layer consisting mainly of Mg(OH)<sub>2</sub> and MgO at the metal/electrolyte interface [2]. Unlike other active metals widely used in industry, such as aluminium and titanium, the

natural oxide film on the surface of magnesium is not uniform. The Pilling–Bedworth ratio of the Mg oxide layer is less than 1. Therefore, it does not provide sufficient corrosion protection and, as a result, limits the use of pure magnesium [1, 3–5].

Optimization of the composition and microstructure of magnesium alloys is one of the ways to increase their corrosion resistance and improve their physical and mechanical properties. Aluminium-containing magnesium alloys of the AZ series (the Mg–Al–Zn system) have received the widest industrial application. Alloying of magnesium with aluminium leads to a decrease in the corrosion rate and an increase in tensile strength, which is due to the formation of the Mg<sub>17</sub>Al<sub>12</sub> β-phase [6, 7], as well as the Al–Mn and Al–Zn phases [8]. An increase in the aluminium content in the alloy from 1 to 5 wt.% leads to the formation of equiaxed grains of the alloy and a decrease in their size. In a corrosive medium, the formed β-phase is characterized by a more electropositive potential compared to the alloy matrix, which can contribute to the occurrence of local corrosion spots [9]. Additional alloying with zinc (up to 1 wt.%) enhances the corrosion resistance and strength of the alloys at room temperature [8].

The AZ31 alloy is one of the most used alloys of the Mg–Al–Zn type. It was shown [10], that heat treatment of the AZ31 alloy leads to the formation of a more homogeneous microstructure with a low dislocation density. Despite the improvement of the corrosion resistance of the alloy, it does not adequately solve the problem of rapid corrosion.

✉ Maria A. Osipenko  
marikaosipenko@gmail.com

✉ Dzmitry S. Kharytonau  
Dmitry.Kharitonov@ikifp.edu.pl

<sup>1</sup> Department of Physical, Colloid, and Analytical Chemistry, Belarusian State Technological University, Minsk 220006, Belarus

<sup>2</sup> Department of Chemistry, Electrochemical Production Technology, and Materials for Electronic Equipment, Belarusian State Technological University, Minsk 220006, Belarus

<sup>3</sup> Institute of Materials Science, Silesian University of Technology, Katowice, PL 40-019, Poland

<sup>4</sup> Jerzy Haber Institute of Catalysis and Surface Chemistry, Polish Academy of Sciences, Krakow, PL 30-239, Poland

A more reliable way to protect Mg alloys from corrosion is to use soluble inhibitors. To provide effective inhibition of Mg alloy corrosion, a fast interaction kinetics of the inhibitor with the metal surface is necessary to suppress the anodic dissolution of the Mg matrix and the cathodic activity of surface constituents. Chromium(VI) compounds have proven to be effective corrosion inhibitors for magnesium and aluminium alloys, carbon steel, zinc, and magnesium alloys. However, due to toxicity and carcinogenicity, the use of these compounds is limited and strictly regulated. Recently, more environmentally friendly alternatives to Cr(VI) compounds have been extensively examined [11, 12]. Such inhibitors as inorganic oxyanions, e.g., aqueous vanadate, molybdate, permanganate, and tungstate, have shown promising performance for suppressing corrosion of Al alloys in NaCl media [13–19]. However, limited knowledge on the use of such inhibitors for the corrosion protection of Mg alloys has been gained in the scientific literature [20]. Recently, the group of Buchheit et al. has examined the inhibitive effect of vanadate and selenite on the Mg alloy AZ31 [21–23]. They have shown that these anions can effectively retard the corrosion attack of the AZ31 alloy by creating insoluble surface passive films. In our recent studies [24, 25], we have examined the mechanism of corrosion inhibition of the AZ31 and the WE43 (Mg–Y–Nd–Zr) alloy by sodium molybdate. Molybdate ions, being adsorbed on the surface of these alloys, form a protective layer of oxides and hydroxides of molybdenum of mixed valence Mo(V)–Mo(VI), which leads to predominant inhibition of the anodic reaction of the corrosion process. One of the possible solutions is to use strong oxidizers, which can rapidly react with the surface to form a protective passive layer. In this regard, the use of potassium permanganate might be promising. It is often used in the development of protective conversion coatings on steel, aluminium, and magnesium alloys with protection ability similar to that of chromate [17, 26–29]. Due to its high solubility in aqueous solutions and high reduction rate, as well as excellent protective ability of the oxide compounds formed in near-neutral media, potassium permanganate can also be effectively used for magnesium alloys as a corrosion inhibitor. Madden and Scully [13] reported that in the case of the AA2024-T351, permanganate acts as a complex ionic inhibitor that is more beneficial when present as a pre-treatment compared to an ionic species addition. However, del Olmo et al. [30] recently reported the use of permanganate as an effective active corrosion inhibitor loaded into layered double hydroxide coating on the AA2024-T3 Al alloy. Therefore, permanganate can be used to combine both pre-treatment and active corrosion protection schemes. Despite the pre-treatment stage of the conversion treatment by permanganate being extensively examined, no detailed examination on the active corrosion protection of Mg alloys by permanganate in the presence of chloride ions has been reported in the literature

[12]. The aim of this study was to investigate the corrosion inhibition of the AZ31 magnesium alloy by potassium permanganate in 0.05 M NaCl solutions in conditions where permanganate acts as an active inhibitor. As the inhibitor performance strongly depends on its concentration, 0.05 M NaCl solutions containing 0.01–0.150 mol/dm<sup>3</sup> of potassium permanganate have been examined, and a possible mechanism of its action has been proposed.

## Experimental

Samples of the magnesium alloy AZ31 with sizes 10 mm × 10 mm × 5 mm were used in all experiments. The nominal elemental composition of the AZ31 alloy is presented as follows (wt.%): 3.8–5.0% Al, 0.8–1.5% Zn, 0.3–0.7% Mn, and balance Mg. Prior to experiments, the samples were mechanically polished in absolute ethanol with the final sandpaper grit of P1200.

Corrosion experiments were performed at least in triplicate in a 0.05 M NaCl aqueous solution serving as a reference medium. The KMnO<sub>4</sub> inhibitor was added to the reference solution in amounts from 0.01 to 0.15 mol/dm<sup>3</sup> without further pH adjustment. A PGSTAT 302N potentiostat/galvanostat (Metrohm Autolab) equipped with an FRA32M impedance module was used in electrochemical experiments. A saturated silver–silver chloride electrode was used as a reference electrode, and a platinum mesh was used as a counter electrode. Before all electrochemical tests, the samples were exposed to the examined solutions for 30 min without any perturbation. Afterwards, the open-circuit potential (OCP) was monitored for 1000 s. In all examined solutions, this time was enough for potential stabilization. Potentiodynamic polarization curves were recorded in the potential range from –300 to +700 mV vs. the OCP with the potential sweep rate of 1 mV/s. Parameters of cathodic and anodic electrochemical processes were calculated using Nova 2.1.5 software. The polarization resistance,  $R_p$ , was calculated from the results of small amplitude linear polarization resistance measurements with a linear potential sweep of 1 mV/s in the overpotential range of ± 10 mV from the OCP. The  $R_p$  was calculated using the equation:

$$R_p = \Delta E / \Delta i_{\Delta E \rightarrow 0}, \quad (1)$$

where  $\Delta E$  is the difference in the electrode potential and  $\Delta i_{\Delta E \rightarrow 0}$  is the difference in the current density when  $\Delta E$  strives towards 0.

Electrochemical impedance spectroscopy (EIS) spectra were recorded in the frequency range from 100 kHz to 0.01 Hz with an oscillation amplitude of 10 mV. Spectra analysis, selection of equivalent circuits, and calculation of the parameters of their elements were performed using the ZView 3.2c

software. The protective effect of the inhibitor was calculated from the electrochemical data using the following relations:

$$IE1, \% = \frac{i_{\text{corr}}^0 - i_{\text{corr}}}{i_{\text{corr}}^0} \quad (2)$$

where  $i_{\text{corr}}^0$  and  $i_{\text{corr}}$  are corrosion current densities in the solution without and with the inhibitor, respectively.

$$IE2, \% = \frac{1/R_p - 1/R_p^0}{1/R_p} \quad (3)$$

where  $R_p^0$  and  $R_p$  are polarization resistances in the solution without and with the inhibitor, respectively.

To determine the amount of hydrogen gas released during the corrosion of the AZ31 alloy, a lab-made setup consisting of two connected burettes filled with distilled water was used. A test tube with 60 ml of the working solution was hermetically attached to the upper side of one of the burettes, into which the preliminarily polished test sample was placed. After the end of the experiment, the burettes were moved to the same level of liquid. The volume of released hydrogen was determined as the arithmetic mean of the change in the liquid level in each of the burettes. The protective effect of the inhibitor was calculated using the following formula:

$$IE3, \% = \frac{V_{H_2}^0 - V_{H_2}}{V_{H_2}^0} \quad (4)$$

where  $V_{H_2}^0$  and  $V_{H_2}$  are volumes of released hydrogen in solutions without and with the inhibitor, respectively.

The microstructure and elemental composition of the alloy surface before and after corrosion testing were studied by scanning electron microscopy (SEM) and energy-dispersive X-ray microanalysis (EDX) using a Hitachi SU8000 and a JEOL JSM-7500F microscopes equipped with chemical X-ray microanalysis modules.

The analysis of the examined surfaces after corrosion tests by confocal Raman spectroscopy was performed using a Jobin–Yvon T64000 spectrometer. The spectra were taken with an Ar<sup>+</sup> laser (wavelength of 514.5 nm) and a power of 5 mW. The accumulation time was 2 × 120 s. Optical images of the surface were taken on a high-resolution 4 K Keyence digital optical microscope of the VHX-S7000 series.

## Results and discussion

### Corrosion experiments

To evaluate the inhibitive effectiveness of permanganate ions, polarization, EIS, and hydrogen evolution experiments were performed. Potentiodynamic polarization curves of the

AZ31 samples in 0.05 M NaCl (Fig. 1, Table 1) showed that potassium permanganate affects both cathodic and anodic slopes of polarization curves. The addition of 0.01 mol/dm<sup>3</sup> KMnO<sub>4</sub> inhibitor increased the modulus of the Tafel slopes of both anodic and cathodic branches of polarization curves. A further increase in the concentration of the KMnO<sub>4</sub> inhibitor in the solution to 0.05 mol/dm<sup>3</sup> resulted in ca. half decrease of the Tafel slope, which remained almost constant with a further increase in the inhibitor concentration in the solution. The minimal values of the Tafel slopes were observed in 0.05 M NaCl solution additionally containing 0.15 mol/dm<sup>3</sup> of the inhibitor. As the addition of the inhibitor affected the kinetics of both cathodic and anodic processes, potassium permanganate showed a mixed-type inhibitor behaviour.

Electrochemical parameters of corrosion of the AZ31 magnesium alloy in the examined media (corrosion potential,  $E_{\text{corr}}$ , and corrosion current density,  $i_{\text{corr}}$ ) were calculated based on the analysis of the Tafel regions (Table 1). A gradual shift of the corrosion potential to the electro-positive region from −1.44 to −1.19 V was observed with an increase in the KMnO<sub>4</sub> concentration in the solution from 0 to 0.15 mol/dm<sup>3</sup>. This may indicate the formation of a surface protective layer of the inhibitor. Calculated values of  $i_{\text{corr}}$  in the reference solution without the inhibitor were  $(1.1 \pm 0.05) \times 10^{-5}$  A/cm<sup>2</sup>. The introduction of 0.01 mol/dm<sup>3</sup> of potassium permanganate into the solution resulted in an increase in the corrosion current density, which is consistent with the results of other studies on oxyanions as corrosion inhibitors [12, 24, 25]. Such a decrease in the corrosion resistance of the AZ31 alloy is explained by only partial hindering of the active corrosion

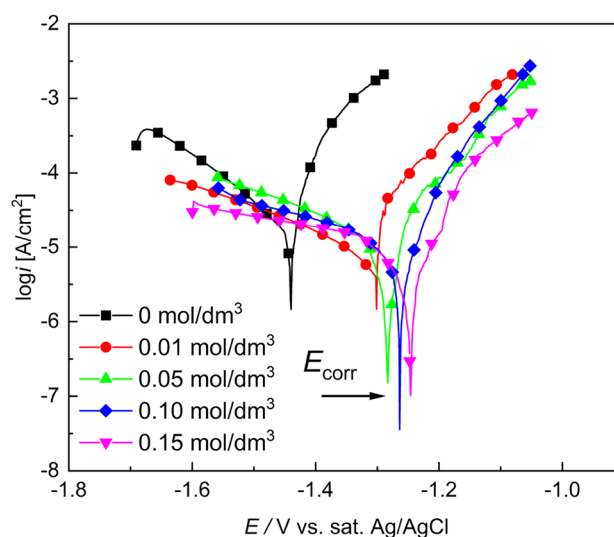


**Fig. 1** Potentiodynamic polarization curves of AZ31 alloy in 0.05 M NaCl solution containing 0.01–0.15 mol/dm<sup>3</sup> of KMnO<sub>4</sub>

**Table 1** Electrochemical parameters of corrosion of AZ31 alloy in 0.05 M NaCl solution containing varying amounts of  $\text{KMnO}_4$  inhibitor extracted from potentiodynamic polarization

Concentration of $\text{KMnO}_4/\text{mol/dm}^3$	$b_c/\text{mV/dec}$	$b_a/\text{mV/dec}$	$i_{\text{corr}}/\text{A/cm}^2$	$E_{\text{corr}}/\text{V}$	$IE1/\%$
0	180	49	$(2.4 \pm 0.7) \times 10^{-5}$	$-1.44 \pm 0.03$	–
0.01	388	85	$(2.5 \pm 0.9) \times 10^{-5}$	$-1.30 \pm 0.02$	–
0.05	147	47	$(6.0 \pm 1.1) \times 10^{-6}$	$-1.27 \pm 0.03$	72
0.10	120	42	$(4.8 \pm 0.3) \times 10^{-6}$	$-1.24 \pm 0.07$	80
0.15	113	39	$(2.2 \pm 0.6) \times 10^{-6}$	$-1.23 \pm 0.1$	91

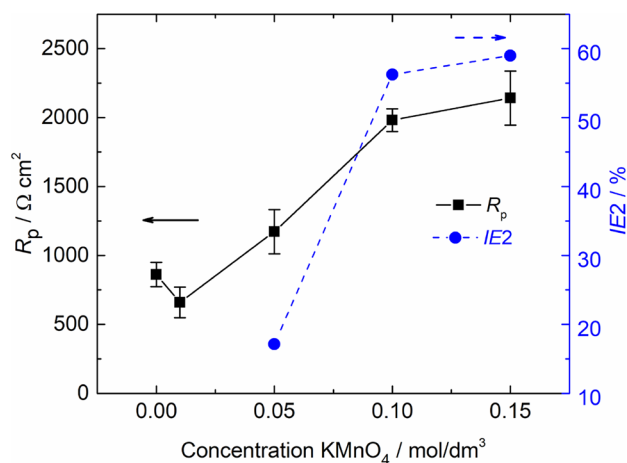
sites by small amounts of the permanganate inhibitor. As a result, corrosion activity of some individual active areas of the surface (cathodic and/or anodic regions) is hindered, while uncovered surface areas remain active, which causes an increase in current density and corrosion rate [31]. At the same time, microgalvanic couples can be formed between surface areas covered with a layer of corrosion products and/or inhibitor to varying degrees, which enhance the propensity to electrochemical corrosion. Similar trends have been previously reported while implementing molybdate inhibitor  $\text{Na}_2\text{MoO}_4$  for corrosion protection of WE43 and AZ31 alloys [24, 25]. In addition, partial screening of the surface leads to an increase in the true current density on the uncovered surface areas, which also contributes to the anodic oxidation of the alloy. In turn, in the solutions containing 0.05–0.15  $\text{mol/dm}^3$  of the permanganate inhibitor,  $i_{\text{corr}}$  decreased significantly. The smallest values of  $i_{\text{corr}}$  ( $1.3 \pm 0.3) \times 10^{-6}$   $\text{A/cm}^2$  were observed in solutions containing 0.15  $\text{mol/dm}^3$  of potassium permanganate. With an increase in the concentration of inhibitor from 0.05 to 0.15  $\text{mol/dm}^3$  in 0.05 M NaCl solutions, the inhibition efficiency  $IE1$  calculated by Eq. (2) increased from 72 to 91%, respectively. This indicates that the manganese-based inhibitor can effectively protect the surface of the AZ31 magnesium alloy from the studied corrosive environment.

The inhibitive effect of the inhibitor was also evaluated based on the values of the polarization resistance,  $R_p$ . The results of the small amplitude linear sweep voltammetry measurements are presented in Fig. 2. The dependence of  $R_p$  calculated by Eq. (1) and, consequently,  $IE2$  calculated by Eq. (3), on the concentration of the inhibitor in the solution, had similar trend with  $i_{\text{corr}}$  and  $IE1$ . The  $R_p$  decreased in the solution containing 0.01  $\text{mol/dm}^3$  of potassium permanganate and gradually increased in the solutions containing a higher amount of the inhibitor. The calculated values of  $IE2$  are 18, 56, and 59% at  $\text{KMnO}_4$  concentrations of 0.05, 0.10, and 0.15  $\text{mol/dm}^3$ , respectively.

The results of the EIS measurements in the form of Nyquist plots are presented in Fig. 3. In all examined solutions, the Nyquist spectra showed a similar appearance with two time constants. The time constant of the

capacitive nature was associated with the adsorption of permanganate ions and corrosion products on the Mg substrate, the capacitance of the formed film, and charge transfer resistance [32]. It appears in the spectra in the form of a distorted capacitive loop. The second time constant in the low-frequency region is of inductive nature and corresponds due to the adsorption of ionized intermediates on the alloy surface during corrosion [25, 33]. In Nyquist plots, it appears in the form of a distorted inductive loop with positive values of  $Z''$ . Similar to the above-described results, it can be seen that the smallest radius of the impedance spectra, i.e. the lowest corrosion resistance, was recorded in 0.05 M NaCl solution additionally containing 0.01  $\text{mol/dm}^3$  of potassium permanganate. This indicates the activation of the corrosion process and supports the assumption that this amount of  $\text{KMnO}_4$  is insufficient for the formation of a continuous protective film on the AZ31 surface.

To quantitatively interpret the obtained spectra, we used the equivalent circuit shown as an inset to Fig. 3. In this circuit,  $R_s$  is the solution resistance;  $R1$  is the resistance of the surface film of the adsorbed inhibitor or the layer of corrosion products;  $R2$  is the charge transfer resistance;  $\text{CPE1}$  is the constant phase element characterizing the protective film

**Fig. 2** Polarization resistance of AZ31 alloy in 0.05 M NaCl solution containing 0.01–0.15  $\text{mol/dm}^3$  of  $\text{KMnO}_4$

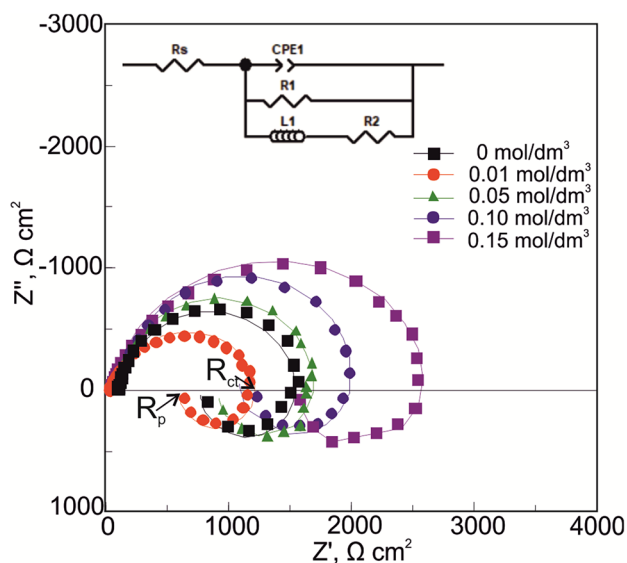


**Fig. 3** Nyquist EIS plots in 0.05 M NaCl solution without and with varying amounts of  $\text{KMnO}_4$  inhibitor. The symbols are experimental data, and the lines are the results of curve fitting using the equivalent circuit shown as an inset

capacitive response;  $L$  is the inductance. The constant phase element (CPE) was used to simulate a capacitive response of the system, since the surface of the samples was characterized by pronounced inhomogeneity. The fitting results are shown in Table 2.

The graphical analysis of the Nyquist spectra showed that the intersection of the obtained spectra with the abscissa axis is possible at two points. In this case, the first intersection in the frequency range of  $100\text{--}10^{-1}$  Hz corresponds to the charge transfer resistance  $R_{ct}$ , while the second intersection at frequencies  $f \rightarrow 0$  can be attributed to the polarization resistance  $R_p$ . In this case, the assessment of the protective effect of the inhibitor based on the values of  $R_{ct}$  can lead to the overestimation of the value of the protective effect [33]. In this regard, to calculate the efficiency of corrosion inhibition of the AZ31 alloy with potassium permanganate, the  $R_p$  values were used. For the proposed equivalent circuit,  $R_p$  was calculated by the following equation:

$$\frac{1}{R_p} = \frac{1}{R_1} + \frac{1}{R_2} \tag{5}$$

The inhibition effect calculated from the  $R_p$  values extracted from the EIS data are 25, 31, and 43% at the concentration of the inhibitor in a solution of 0.05, 0.10, and 0.15 mol/dm<sup>3</sup>, respectively (Table 2).

Figure 4a shows the volume of released hydrogen during corrosion of the AZ31 alloy in 0.05 M NaCl solutions with different concentrations of potassium permanganate depending on the immersion time. For all examined solutions, the amount of released hydrogen gradually increases with increasing the immersion time up to 168 h. The amount of released hydrogen in 0.05 M NaCl solution without the inhibitor was significantly greater than in solutions containing potassium permanganate. The introduction of potassium permanganate into the corrosive environment led to a sharp decrease in the volume of released hydrogen. This is due to the formation of a manganese-containing protective film on the surface of the magnesium alloy, which prevents the corrosion process, accompanied by the release of hydrogen. Within the same immersion duration, an increase in the concentration of permanganate ions from 0.01 to 0.15 mol/dm<sup>3</sup> contributed to a slight decrease in the amount of released hydrogen gas. The inhibition effect calculated by Eq. (4) is shown in Fig. 4b. A slight decrease in the  $IE_3$  in solutions with a low inhibitor content (0.01–0.05 mol/dm<sup>3</sup>) after 24 h of exposure is explained by a non-uniform inhibitor film on the surface, which do not provide a reliable inhibition. After 36 h of exposure, the calculated values of  $IE_3$  are higher than 90% for all examined concentrations of the inhibitor (Fig. 4b). A slight decrease in the inhibition effect during long-term exposure of samples in 0.05 M NaCl solutions containing  $\text{KMnO}_4$  is explained by a gradual degradation of the surface protective layers formed on the surface of the samples.

It should be noted that the inhibitive effect of the permanganate inhibitor for all examined concentrations, calculated based on the data of electrochemical studies and the amount of released hydrogen, varied significantly. This difference was especially prominent in long-time studies. Most probably, the holding interval before the electrochemical tests (ca.

**Table 2** Results of fitting EIS spectra of the AZ31 alloy in 0.05 M NaCl solutions containing varying amounts of permanganate inhibitor

Concentration of $\text{KMnO}_4$ , mol/dm <sup>3</sup>	$R_s$ , $\Omega \text{ cm}^2$	$R_1$ , $\Omega \text{ cm}^2$	$R_2$ , $\Omega \text{ cm}^2$	$\text{CPE1}, \Omega^{-1} \text{ cm}^{-2} \text{ s}^n$	$n_1$	$L$ , H $\text{ cm}^2$	$R_p$ , $\Omega \text{ cm}^2$	$IE_2$ , %
0	$97.9 \pm 1.8$	$1464 \pm 41.5$	$1146 \pm 35.8$	$(1.33 \pm 0.01) \cdot 10^{-5}$	$0.92 \pm 0.01$	$1335 \pm 70.8$	642.8	–
0.01	$23.1 \pm 2.1$	$1203 \pm 46.9$	$900 \pm 25.3$	$(2.81 \pm 0.21) \cdot 10^{-6}$	$0.86 \pm 0.01$	$1035 \pm 55.8$	514.8	–
0.05	$55.8 \pm 1.8$	$1723 \pm 47.1$	$1710 \pm 52.6$	$(2.41 \pm 0.22) \cdot 10^{-5}$	$0.91 \pm 0.1$	$2087 \pm 15.6$	858.2	25
0.10	$100.6 \pm 2.3$	$1905 \pm 72.5$	$1810 \pm 173.1$	$(1.37 \pm 0.05) \cdot 10^{-5}$	$0.92 \pm 0.02$	$2387 \pm 38.1$	928.1	31
0.15	$135.0 \pm 1.7$	$2405 \pm 60.6$	$2100 \pm 21.3$	$(1.99 \pm 0.12) \cdot 10^{-5}$	$0.89 \pm 0.01$	$2580 \pm 33.9$	1121.1	43



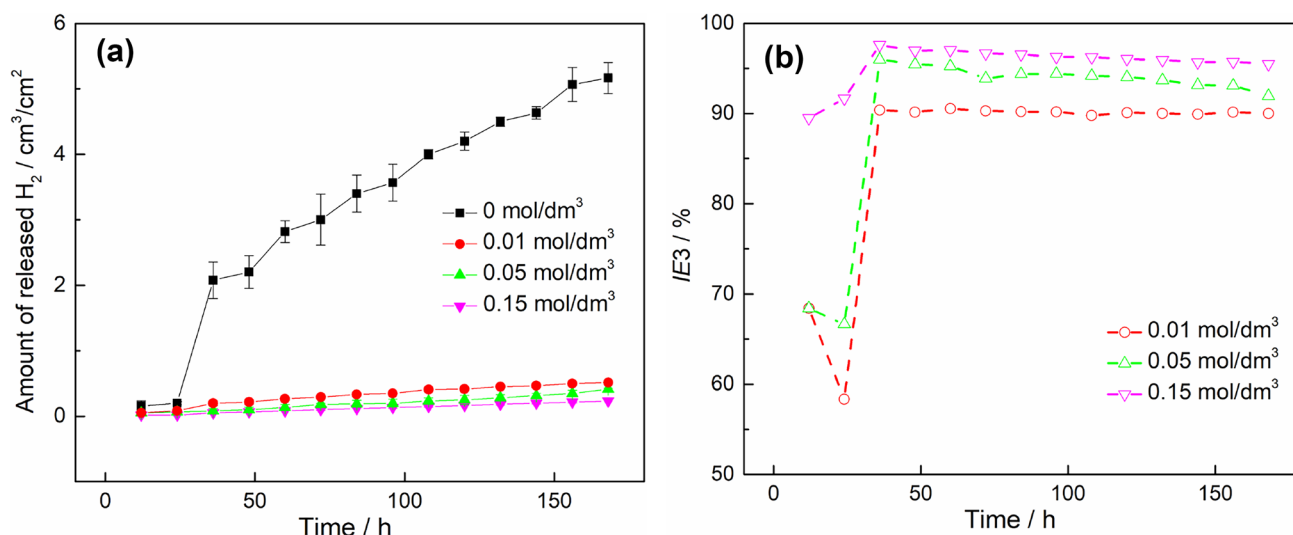


**Fig. 4** Amount of released hydrogen (a) and inhibition effect (b) during exposure of the AZ31 alloy in 0.05 M NaCl with varying amounts of permanganate inhibitor

47 min) was not enough to form a continuous surface protective film in the solutions with a low content of  $\text{KMnO}_4$ . In addition, during long-term corrosion tests, a layer of magnesium corrosion products forms on the surface of the samples, which can also prevent further corrosion damage.

Thus, the performed corrosion experiments revealed that in 0.05 M NaCl solution, potassium permanganate provides reliable corrosion inhibition in the amount of  $0.15 \text{ mol/dm}^3$ . Therefore, further studies were performed using the samples exposed to 0.05 M NaCl solutions containing  $0.15 \text{ mol/dm}^3$   $\text{KMnO}_4$ .

### Surface analysis

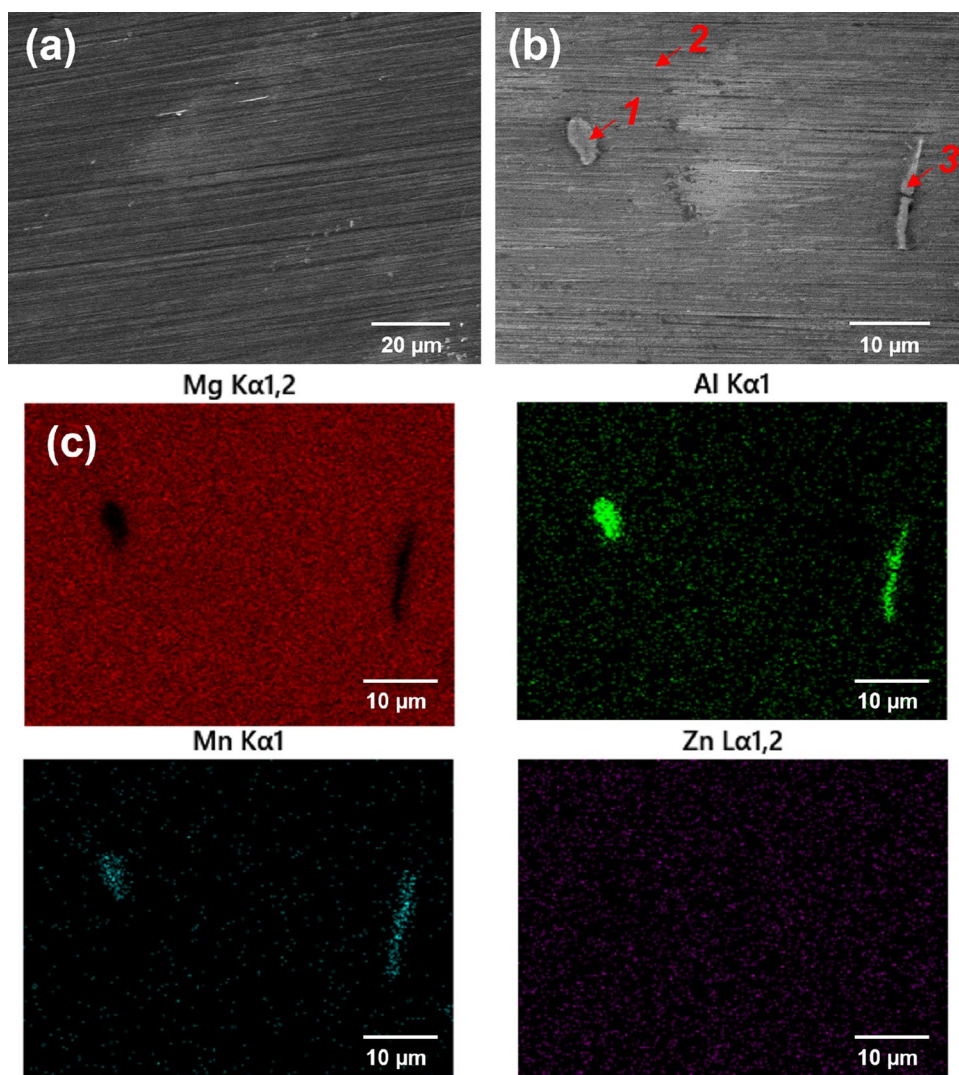
Figure 5 shows the SEM micrographs of the microstructure of the as-polished AZ31 alloy. The microstructure of the alloy consists of an  $\alpha$ -Mg matrix and two characteristic types of intermetallic particles (IMPs). The first type represents polyhedral particles with sizes of about tens of microns. The second type are rectangle-shaped IMPs with the longest side around  $10 \mu\text{m}$ . These particles usually formed prolonged IMPs agglomerates consisting of several smaller IMPs located very close to each other. Both types of IMPs were randomly distributed in the alloy matrix. Based on the point EDX analysis (Fig. 5b and Table 3), these IMPs are of Al–Mn type, which agrees well with the literature and our previous data [24, 34]. Some analysed phases also had a minor fraction of Zn, which is typical for Al–Mg–Zn phases [8]. However, their exact stoichiometry cannot be reliably detected based on the EDX analysis. Therefore, only elemental composition was considered. The EDX maps (Fig. 5c) showed that Al and Mn are uniformly distributed over the

surface of IMPs and Mg matrix. In the case of Zn, its distribution was almost uniform over the whole examined region.

The analysis of the microstructure of the surface of the AZ31 magnesium alloy after corrosion experiments is summarized in Fig. 6. After 5 min of corrosion in 0.05 M NaCl solution without the inhibitor, the surface of the AZ31 alloy is already covered by a visible layer of corrosion products (Fig. 6a). The IMP/matrix interface remained almost intact, while the corrosion attack was concentrated on the alloy matrix. After 30 min of the corrosion test, the surface was covered by a well-visible layer of corrosion products (Fig. 6b). The location of the corrosion attack concentrated around IMPs regions, while large regions of the alloy matrix remained almost uncovered. Corrosion extended after 1 h of exposure to 0.05 M NaCl solution, and the surface was partially covered by a thick layer of corrosion products. Moreover, numerous sites of a prominent local corrosion attack can be detected (Fig. 6c). After 24 h of exposure, almost entire surface was covered with a layer of corrosion products (Fig. 6d).

In the case when  $0.15 \text{ mol/dm}^3$  of potassium permanganate were added into 0.05 M NaCl solution, corrosion of the AZ31 alloy was significantly suppressed. After 5 min of corrosion experiments (Fig. 6e), the surface was almost intact, and after 30 min (Fig. 6f), some spots on the surface were covered by a layer of corrosion products. After 1 h of exposure, an almost uniform manganese-containing protective film was formed on the surface (Fig. 6g, Table 3). Several cracks and local defects in the structure of the formed film can be explained by the concentration of internal microstresses in these areas of the formed protective layer. The formed protective layers are characterized by inhomogeneity,

**Fig. 5** SEM micrographs of the surface of as-polished AZ31 magnesium alloy (**a**, **b**) and EDX elemental distribution maps (**c**) of the surface region (**b**). The elemental composition of point EDX analysis marked in **b** is given in Table 3



which may be due to the heterogeneous structure of the alloy, consisting of the  $\alpha$ -Mg matrix and IMPs [8, 35], which are active centres of the formation of manganese-containing films.

The results of the elemental analysis of the surface of the AZ31 alloy after corrosion tests are listed in Table 3. In every case, the EDX analysis of two characteristic areas of the surface was performed (the spot number in Table 3 corresponds to the surface area marked in Fig. 6). After 5 min of corrosion in 0.05 M NaCl without the inhibitor, the relative composition of the alloy matrix remained close to the as-polished surface, with a small increase in the fraction of oxygen, suggesting the formation of a layer of corrosion products on the surface. In the case of IMP (point 4 in Table 3 and Fig. 6a), a relative decrease of Mg fraction compared to the as-polished surface was observed, which might suggest the selective dissolution of Mg from these constituents. Oppositely, after 30 min of corrosion exposure, the relative fraction of Mg in analysed IMPs increased, suggesting their

partial coverage by a layer of corrosion products in the form of hydrated magnesium oxide and selective dissolution of Al and Mn. After 1 h of exposure to 0.05 NaCl solution, the main fraction of the surface composition was magnesium and oxygen, with almost complete removal of Al, Zn, and Mn from the surface of the samples both in matrix and IMPs regions. An increase in the exposure time to 24 h led to a further decrease in the aluminium content in the composition of surface films, which may be due to the transition of cathode IMPs into the solution as a result of local anodic dissolution of magnesium at the phase boundary Mg-matrix|IMP, as well as chemical dissolution of Al from IMPs and alloy matrix due to a pH increase in the near-surface layer. The occurrence of this process is clearly visible in SEM images after 24 h of corrosion tests (Fig. 6d).

In the case of 0.05 M NaCl solution containing 0.15 mol/dm<sup>3</sup> of the permanganate inhibitor, the weight content of manganese in the composition of surface films compared to

**Table 3** Elemental composition of the surface of AZ31 alloy before and after corrosion tests based on the results of EDX analysis

Sample	Point of analysis (Figs. 5 and 6)	Elemental composition, wt.%					
		Mg	Al	Zn	Mn	O	Cl
As-polished surface	1	11.3	52.0	–	36.1	0.6	–
	2	93.0	4.5	1.1	–	1.4	–
	3	10.6	36.3	0.4	50.7	2.0	–
0.05 M NaCl	Exposure time 5 min						
	4	4.9	33.0	–	55.0	7.1	–
	5	93.3	1.7	0.8	0.6	3.6	–
	Exposure time 30 min						
	6	93.5	2.3	0.6	–	3.6	–
	7	32.5	24.1	0.6	33.9	8.9	–
	Exposure time 1 h						
	8	38.3	6.9	–	–	46.9	7.9
	9	57.8	4.6	–	–	30.8	6.8
	Exposure time 24 h						
	10	39.6	4.8	–	–	50.4	5.2
11	61.6	4.1	–	–	25.4	8.9	
0.05 M NaCl + 0.15 mol/dm <sup>3</sup> KMnO <sub>4</sub>	Exposure time 5 min						
	12	3.2	28.1	–	65.4	3.3	–
	13	94.4	2.9	0.5	0.4	1.8	–
	Exposure time 30 min						
	14	1.3	26.5	1.1	65.7	5.5	–
	15	92.5	3.0	0.8	1.1	2.7	–
	Exposure time 1 h						
	16	74.4	2.0	–	11.8	11.7	–
	17	80.3	0.7	–	9.8	9.2	–
	Exposure time 24 h						
	18	54.5	0.8	–	28.7	16.0	–
19	26.8	0.7	–	42.5	30.0	–	

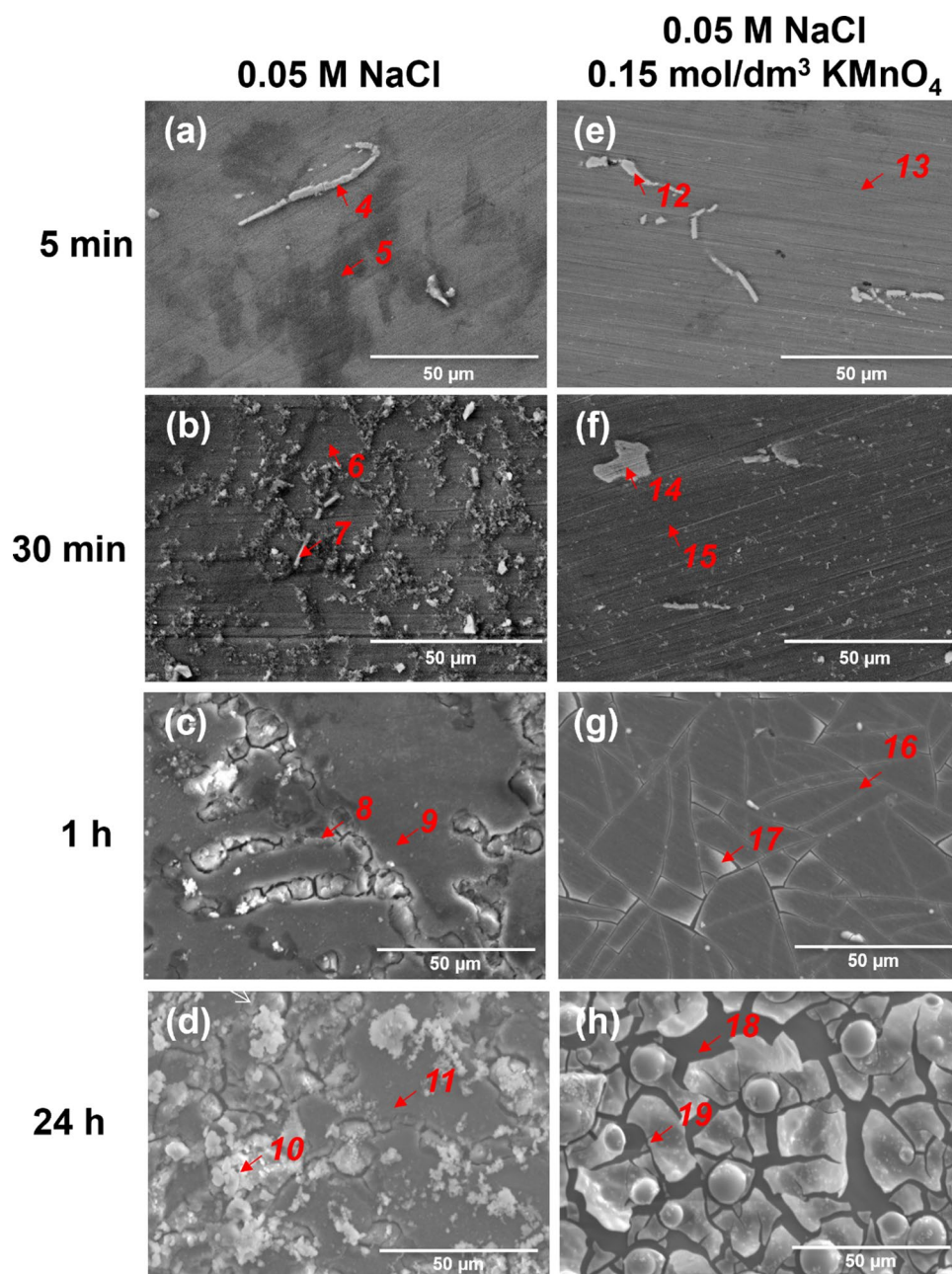
those in the solution without inhibitor increases in all examined exposure times (Table 3). The most notable difference was observed for IMPs regions after 5 and 30 min of exposure, suggesting that the permanganate inhibitor primarily interacts with cathodic IMPs suppressing their electrochemical activity. In this case, a sharp decrease in the aluminium content compared to samples kept in 0.05 M NaCl solution indicate the predominant adsorption of permanganate ions on the surface of cathodic aluminium-containing IMPs, which leads to the shielding of Al by the formed manganese-containing compounds [17, 36]. After 1 and 24 h of exposure, it was not possible to identify IMPs under the formed protective Mn-rich layer. However, a noticeable difference in the elemental composition of two surface areas of the same sample is due to different degrees of surface coverage with corrosion products and manganese compounds. In addition, a different elemental composition can be associated with an inhomogeneous surface microstructure, i.e., with different amounts and compositions of intermetallic particles in the site selected for the point EDX analysis (Fig. 6).

To further study the phase composition of the AZ31 surface after corrosion experiments in permanganate-containing sodium chloride solutions, Raman spectra (Fig. 8) were acquired from the surface areas shown in Fig. 7. Here, we report the results obtained only after 1 and 24 h of corrosion experiments, since surface layers after 5 and 30 min were too thin for registering high-quality spectra and provide their reliable analysis.

After 1 and 24 h of exposure of the AZ31 alloy to 0.05 M NaCl solution without the permanganate inhibitor, two Raman bands at 280 and 443 cm<sup>-1</sup> were identified as E<sub>g</sub>(T) and A<sub>1g</sub>(T) vibrations characteristic of Mg(OH)<sub>2</sub> [37, 38]. The Raman spectra obtained after 1 h of exposure to 0.05 M NaCl solution additionally containing 0.15 mol/dm<sup>3</sup> of potassium permanganate exhibited peaks at 491, 572, 631, and 670 cm<sup>-1</sup>, which indicated the presence of γ-MnO<sub>2</sub> manganese oxide on the surface [39]. The Raman bands in the range 580–632 cm<sup>-1</sup> are due to symmetrical vibrations of the Mn–O bond, which indicates a well-developed tetragonal structure [40]. Raman bands in the range of 530, 560, and



**Fig. 6** SEM micrographs of the surface of the AZ31 magnesium alloy exposed in 0.05 M NaCl solution without inhibitor (a–d) and with the addition of 0.15 mol/dm<sup>3</sup> of KMnO<sub>4</sub> (e–h). The elemental composition of marked points is given in Table 3

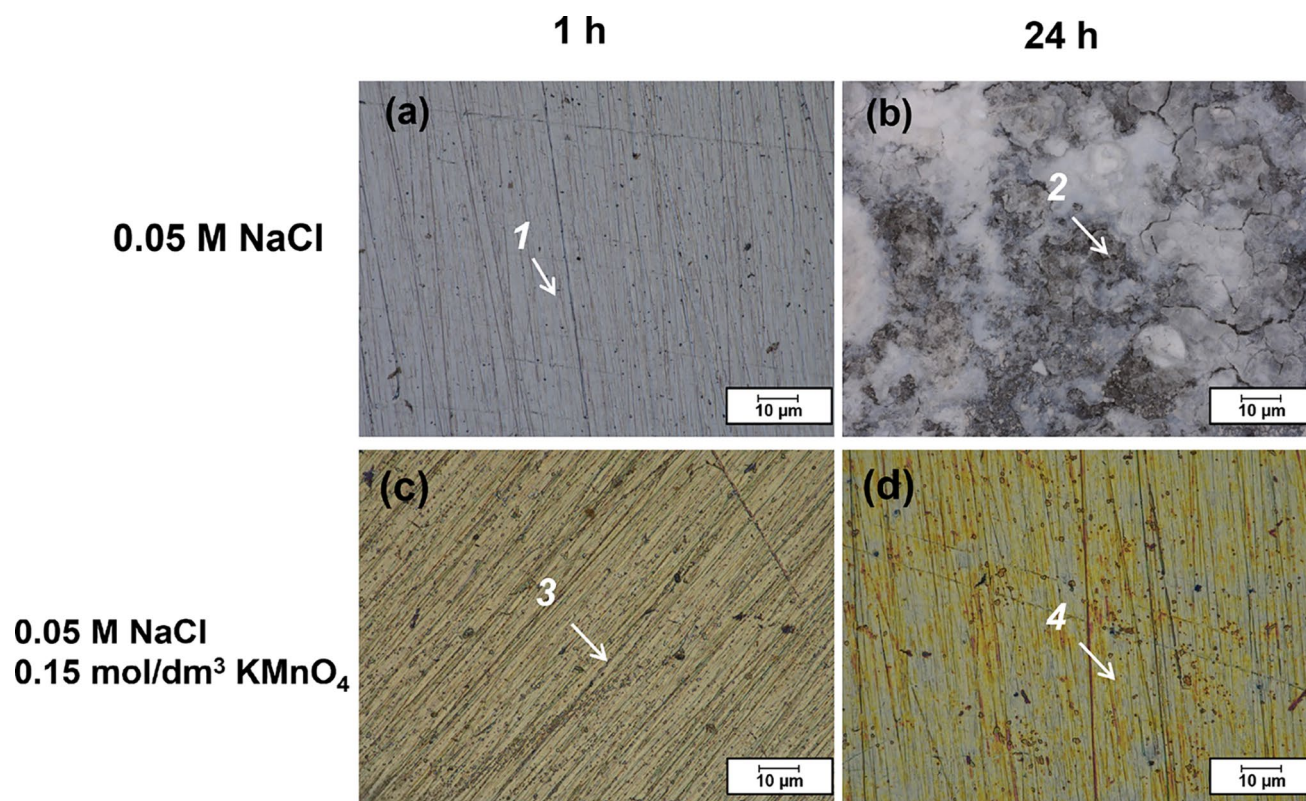


625 cm<sup>-1</sup> were identified as a signal from the trivalent manganese-containing MnOOH [41, 42]. In turn, after 24 h of exposure to manganese-containing solutions, bands assigned to only Mn(IV) compounds were observed in the spectrum.

### Corrosion mechanism

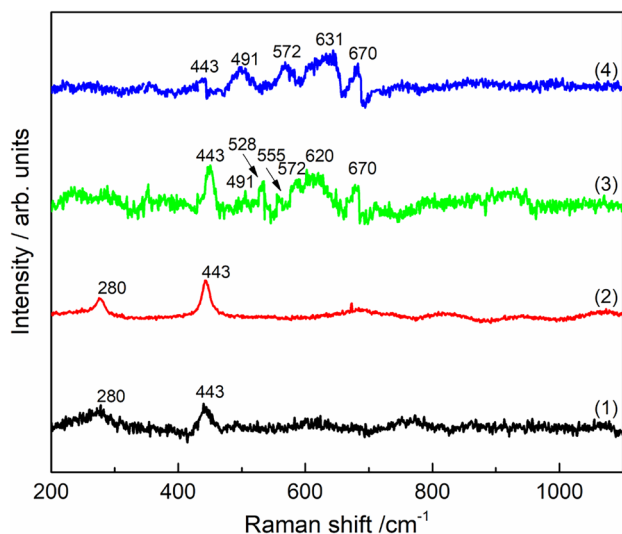
This section aims to summarize the obtained results and provide a description of the corrosion mechanism of the AZ31 alloy in 0.05 M NaCl solutions with and without potassium permanganate. In aqueous solutions, manganese compounds in multiple oxidation states between +7 and +2 can form. Figure 9a shows the calculated equilibrium  $E$ -pH

diagram of Mn compounds in the 0.05 M NaCl solution containing 0.15 mol/dm<sup>3</sup> of KMnO<sub>4</sub>. Potassium permanganate is a strong oxidizer, and at pH above 7 (typical for corrosion of Mg alloys), insoluble oxides or hydroxides of Mn in different oxidation states exist. However, at low pHs, these species can solve to form soluble Mn<sup>2+</sup> species. In the case of the examined system, permanganate ions will interact with the surface of the AZ31 alloy, and the OCP will establish between the metal surface and corrosive medium. The predicted equilibrium speciation diagram at the OCP of -1.22 V vs. sat. Ag/AgCl, which was observed in corrosion experiments (Fig. 1 and Table 2), is calculated in Fig. 9b. It can be seen that at pHs above ca. 8, Mn(OH)<sub>2</sub>



**Fig. 7** Optical photographs of characteristic surface areas of the AZ31 alloy surface after exposure for 1 and 24 h to 0.05 M NaCl solutions without (a, b) and with 0.15 mol/dm<sup>3</sup> of KMnO<sub>4</sub> (c, d). Labels of surface areas correspond to Raman spectra shown in Fig. 8

is the only predictable Mn compound, while at lower pHs, several soluble compounds can form. However, it is important to remember that calculated diagrams show equilibrium



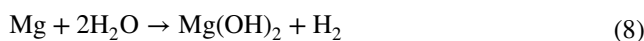
**Fig. 8** Raman spectra of the surface of the AZ31 alloy after exposure for 1 h (1, 3) and 24 h (2, 4) to 0.05 M NaCl solutions without (1, 2) and with 0.15 mol/dm<sup>3</sup> of KMnO<sub>4</sub> (3, 4). Spectra numbers correspond to surface areas shown in Fig. 7

conditions, while examined system strives towards this equilibrium.

Based on the performed experiments, the following mechanism was proposed (Fig. 10). Initially, after immersion of the Mg alloy into the sodium chloride solution, two parallel processes can occur at the Mg-matrix|cathodic IMP interface: the dissolution of the magnesium matrix and hydrogen evolution (Fig. 10a, b) [1, 44–46]:



which can be summarized as:



According to the results of the EDX analysis, a prominent decrease in the surface content of zinc and manganese is observed as the exposure time increases. This may be explained by two reasons. Firstly, the dissolution of the Mg matrix along the boundary of cathodic IMPs promotes their transition into solution. Secondly, alkalization of the solution according to reaction (7) leads to an increase in the solution pH in the near-electrode region. The latter

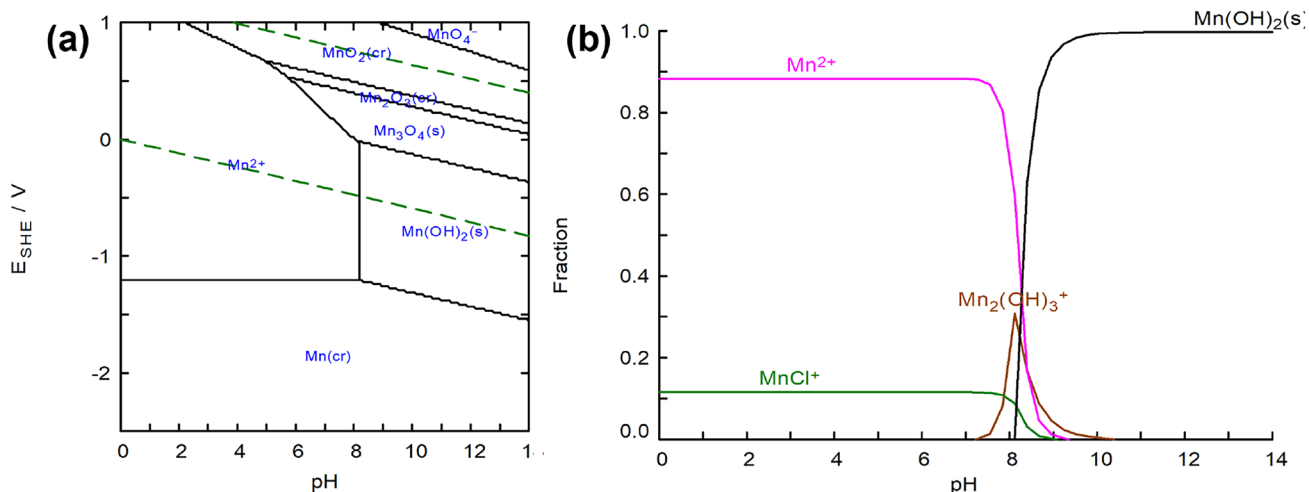


**Fig. 9** *E*-pH (a) and volume fraction (b) diagrams for an aqueous 0.05 M NaCl solution containing 0.15 mol/dm<sup>3</sup> of KMnO<sub>4</sub>. The concentration of Mg<sup>2+</sup> ions was set to 1 mol/dm<sup>3</sup>. The volume fraction data were calculated at a potential of -1.22 V vs. sat. Ag/AgCl to

simulate the OCP of AZ31 in these conditions (Table 2). The green dashed lines in **a** enclose the region of water stability. Diagrams were calculated using the Medusa software [43]

process may occur also due to the dissociation of the resulting magnesium hydroxide:



High pH values, in turn, promote the chemical dissolution of amphoteric zinc and aluminium constituents of the AZ31 alloy, resulting in the formation of complexes (Fig. 10c):

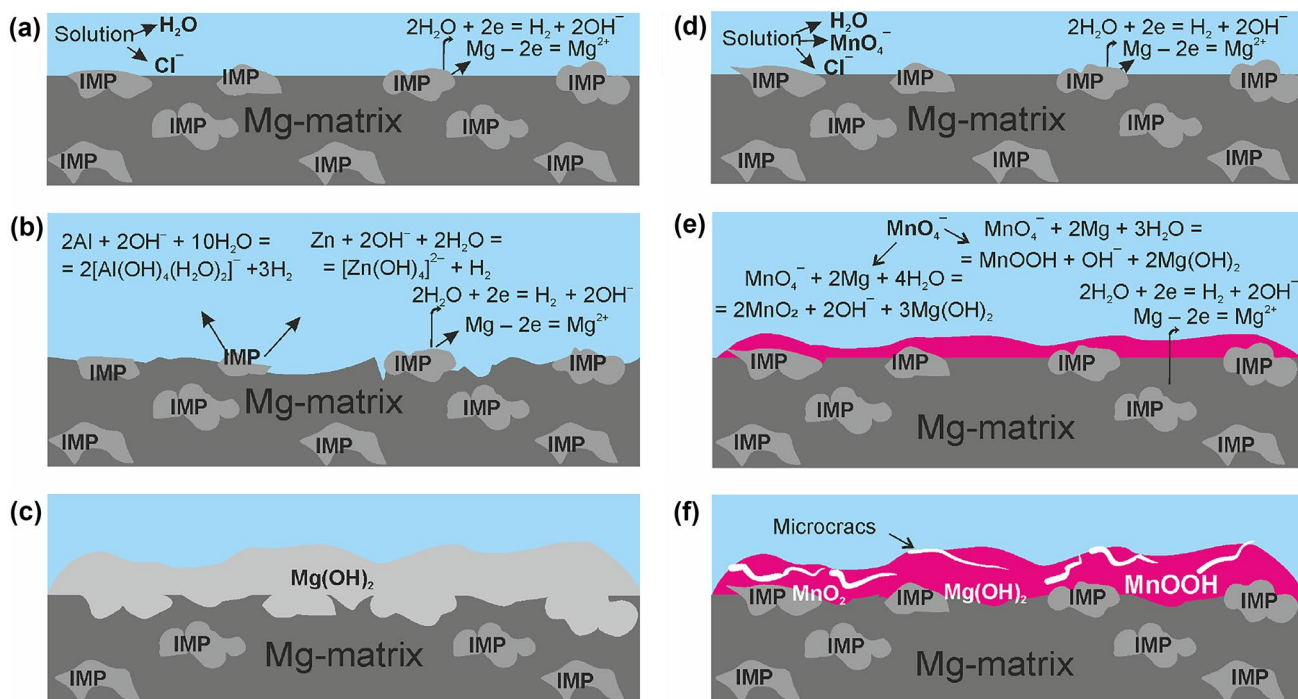
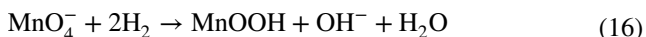
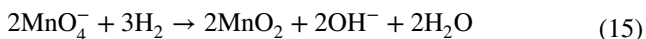
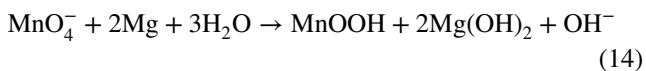
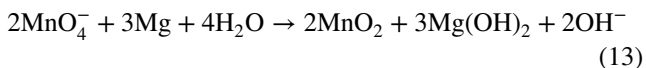


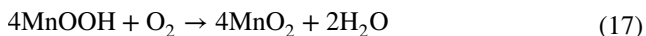
**Fig. 10** A schematic illustration of initiation and propagation of AZ31 alloy corrosion in 0.05 M NaCl solution without (a–c) and with 0.15 mol/dm<sup>3</sup> of molybdate inhibitor (d–f)



As discussed above, IMPs in the microstructure of the AZ31 alloy are cathodic relative to the alloy matrix, which promotes the adsorption of manganese-containing anions on the surface of the AZ31 alloy and their subsequent reduction to manganese(IV) oxide and manganese(III) metahydroxide (Fig. 10d):



As the amount and surface coverage of the alloy surface by corrosion products increases, its shielding occurs (Fig. 10e). During prolonged corrosion attack, manganese metahydroxide, which is part of the protective film, is gradually oxidized by dissolved oxygen to  $\text{MnO}_2$  (Fig. 10f).



## Conclusions

In this work, corrosion of the AZ31 magnesium alloy in 0.05 M NaCl solutions without and with permanganate inhibitor was examined. Permanganate inhibitor provided acceptable levels of inhibition at relatively high concentrations (0.10–0.15 mol/dm<sup>3</sup>). The following conclusions can be drawn:

1. According to electrochemical impedance spectroscopy data, the addition of 0.01 mol/dm<sup>3</sup> of  $\text{KMnO}_4$  into a 0.05 M NaCl solution leads to a decrease in the corrosion resistance of the AZ31 alloy. With a further increase in the content of potassium permanganate in the solution, the protective effect calculated based on the polarization resistance data increases to 26.22, 43.98, and 54.66% at a  $\text{KMnO}_4$  concentration of 0.05, 0.10, and 0.15 mol/dm<sup>3</sup>, respectively.
2. Potentiodynamic polarization studies showed that in a 0.05 M NaCl solution, potassium permanganate behaves as the mixed-type inhibitor. The corrosion current density of the AZ31 alloy in the solution containing 0.01 mol/dm<sup>3</sup> of the inhibitor slightly increased, which indicates low corrosion protection due to only partial coverage of the surface by manganese-containing compounds. The introduction of 0.05–0.15 mol/dm<sup>3</sup> of  $\text{KMnO}_4$  into the corrosive medium leads to a decrease in the corrosion current densities and, consequently, to an increase in the inhibition efficiency, which based on the  $i_{\text{corr}}$  data is 12.0 to 87.0% depending on the inhibitor concentration.

3. The results of Raman spectroscopy showed that after 1 h of corrosion tests, the formed protective film consists of magnesium hydroxide  $\text{Mg}(\text{OH})_2$  and manganese(III, IV) compounds  $\text{MnO}_2$  and  $\text{MnOOH}$ . With an increase in the exposure time to 24 h, manganese(III) metahydroxide  $\text{MnOOH}$  gradually oxidized to manganese(IV) oxide.
4. The surface analysis of the AZ31 magnesium alloy samples showed that in 0.05 M NaCl solution, corrosion is localized at the Mg-matrix|cathodic IMPs interface, which leads to alkalinization of the solution in the near-surface area, partial detachment of IMPs from the alloy surface, and dissolution of their constituents. In the presence of 0.15 mol/dm<sup>3</sup> of the  $\text{KMnO}_4$  inhibitor in the corrosive medium, the mechanism of corrosion inhibition of AZ31 magnesium alloy by soluble permanganates includes the stage of adsorption of ions on the surface of the cathodic IMPs and reduction to manganese(III,IV) compounds  $\text{MnO}_2$  and  $\text{MnOOH}$  with the formation of a continuous protective film, mainly consisting of magnesium hydroxide and manganese(IV) oxide.

**Acknowledgements** Dzmityr Kharytonau gratefully acknowledges financial support from the National Science Centre (Poland) under research Grant Miniatura no. 2019/03/X/ST4/00749. Irina Kurilo gratefully acknowledges financial support from the Ministry of Education of the Republic of Belarus under grant no. 20212333 “Synthesis and properties of metal implantation biomaterials based on surface-hardened titanium alloys and biodegradable magnesium alloys”. Maria A. Osipenko gratefully acknowledges financial support from the Ministry of Education of the Republic of Belarus under grant no. 20220542 “Kinetic and corrosion mechanisms of magnesium-aluminium alloys in sodium chloride solutions in the presence of manganese(VII) and molybdenum(VI) ions”. Angelika Wrzesińska (Lodz University of Technology, Poland) is gratefully acknowledged for her assistance with Raman measurements.

**Author contribution** Maria A. Osipenko: investigation; data curation, formal analysis, visualization, writing—original draft. Aliaksandr A. Kasach: investigation. Janusz Adamiec: resources, investigation. Małgorzata Zimowska: investigation. Irina I. Kurilo: project administration, funding acquisition, writing—original draft. Dzmityr S. Kharytonau: conceptualization, methodology, investigation, data curation, formal analysis, visualization, validation, funding acquisition, project administration, writing—original draft.

**Data availability** The raw/processed data required to reproduce the findings of this study are available from the corresponding authors upon reasonable request.

## Declarations

**Conflict of interest** The authors declare no competing interests.

**Open Access** This article is licensed under a Creative Commons Attribution 4.0 International License, which permits use, sharing, adaptation, distribution and reproduction in any medium or format, as long as you give appropriate credit to the original author(s) and the source, provide a link to the Creative Commons licence, and indicate if changes were made. The images or other third party material in this article are included in the article's Creative Commons licence, unless indicated



otherwise in a credit line to the material. If material is not included in the article's Creative Commons licence and your intended use is not permitted by statutory regulation or exceeds the permitted use, you will need to obtain permission directly from the copyright holder. To view a copy of this licence, visit <http://creativecommons.org/licenses/by/4.0/>.

## References

- Esmaily M, Svensson JE, Fajardo S et al (2017) Fundamentals and advances in magnesium alloy corrosion. *Prog Mater Sci* 89:92–193. <https://doi.org/10.1016/j.pmatsci.2017.04.011>
- Liu M, Zanna S, Ardelean H et al (2009) A first quantitative XPS study of the surface films formed, by exposure to water, on Mg and on the Mg–Al intermetallics: Al<sub>3</sub>Mg<sub>2</sub> and Mg<sub>17</sub>Al<sub>12</sub>. *Corros Sci* 51:1115–1127. <https://doi.org/10.1016/j.corsci.2009.02.017>
- Kaya AA (2020) A review on developments in magnesium alloys. *Front Mater*. <https://doi.org/10.3389/fmats.2020.00198>
- Tan J, Ramakrishna S (2021) Applications of magnesium and its alloys: a review. *Appl Sci* 11:6861. <https://doi.org/10.3390/app11156861>
- Chen XB, Birbilis N, Abbott TB (2011) Review of corrosion-resistant conversion coatings for magnesium and its alloys. *Corrosion* 67:035005-1-035005-16. <https://doi.org/10.5006/1.3563639>
- Gusieva K, Davies CHJ, Scully JR, Birbilis N (2015) Corrosion of magnesium alloys: the role of alloying. *Int Mater Rev* 60:169–194. <https://doi.org/10.1179/1743280414Y.0000000046>
- Lee YC, Dahle AK, StJohn DH (2000) The role of solute in grain refinement of magnesium. *Metall Mater Trans A* 31:2895–2906. <https://doi.org/10.1007/BF02830349>
- Papenberg NP, Gneiger S, Weißensteiner I et al (2020) Mg-alloys for forging applications—a review. *Materials (Basel)* 13:985. <https://doi.org/10.3390/ma13040985>
- Zhang T, Li Y, Wang F (2006) Roles of  $\beta$  phase in the corrosion process of AZ91D magnesium alloy. *Corros Sci* 48:1249–1264. <https://doi.org/10.1016/j.corsci.2005.05.011>
- Li D-W, Wang H-Y, Wei D-S et al (2020) Effects of deformation texture and grain size on corrosion behavior of Mg–3Al–1Zn alloy sheets. *ACS Omega* 5:1448–1456. <https://doi.org/10.1021/acsomega.9b03009>
- Wierzbička E, Vaghefinazari B, Mohedano M et al (2022) Chromate-free corrosion protection strategies for magnesium alloys—a review: part II—PEO and anodizing. *Materials (Basel)* 15:8515. <https://doi.org/10.3390/ma15238515>
- Vaghefinazari B, Wierzbička E, Visser P et al (2022) Chromate-free corrosion protection strategies for magnesium alloys—a review: part III—corrosion inhibitors and combining them with other protection strategies. *Materials (Basel)* 15:8489. <https://doi.org/10.3390/ma15238489>
- Madden SB, Scully JR (2014) Inhibition of AA2024-T351 corrosion using permanganate. *J Electrochem Soc* 161:C162–C175. <https://doi.org/10.1149/2.075403jes>
- Iannuzzi M, Frankel GS (2007) Mechanisms of corrosion inhibition of AA2024-T3 by vanadates. *Corros Sci* 49:2371–2391. <https://doi.org/10.1016/j.corsci.2006.10.027>
- Kharitonov DS, Ornek C, Claesson PM et al (2018) Corrosion inhibition of aluminum alloy AA6063-T5 by vanadates: microstructure characterization and corrosion analysis. *J Electrochem Soc* 165:C116–C126. <https://doi.org/10.1149/2.0341803jes>
- Kharitonov DS, Dobryden I, Sefer B et al (2020) Surface and corrosion properties of AA6063-T5 aluminum alloy in molybdate-containing sodium chloride solutions. *Corros Sci* 171:108658. <https://doi.org/10.1016/j.corsci.2020.108658>
- Kharitonov DS, Makarova IV, Osipenko MA et al (2020) The deposition mechanism and protective properties of manganese-based conversion coatings on the surface of AD31 aluminum alloy. *Prot Met Phys Chem Surfaces* 56:113–124. <https://doi.org/10.1134/S2070205120010128>
- Kharitonov DS, Osipenko MA, Wrzesińska A et al (2020) Protective action of sodium metavanadate against corrosion of AD31 aluminum alloy in neutral chloride-containing media. *Russ J Phys Chem A* 94:874–879. <https://doi.org/10.1134/S0036024420040068>
- Kwolek P, Dychtoń K, Pytel M (2019) Orthophosphoric acid solutions of sodium orthovanadate, sodium tungstate, and sodium molybdate as potential corrosion inhibitors of the Al<sub>2</sub>Cu intermetallic phase. *J Solid State Electrochem* 23:3019–3029. <https://doi.org/10.1007/s10008-019-04397-0>
- Lamaka SV, Vaghefinazari B, Mei D et al (2017) Comprehensive screening of Mg corrosion inhibitors. *Corros Sci* 128:224–240. <https://doi.org/10.1016/j.corsci.2017.07.011>
- Feng Z, Hurley B, Zhu M et al (2019) Corrosion inhibition of AZ31 Mg alloy by aqueous selenite (SeO<sub>3</sub><sup>2-</sup>). *J Electrochem Soc* 166:C520–C529. <https://doi.org/10.1149/2.0911914jes>
- Feng Z, Hurley B, Li J, Buchheit R (2018) Corrosion inhibition study of aqueous vanadate on Mg Alloy AZ31. *J Electrochem Soc* 165:C94–C102. <https://doi.org/10.1149/2.1171802jes>
- Feng Z, Xu CC, Zhang D, Buchheit R (2021) Corrosion protective film formation on Mg Alloy AZ31 by exposure to dilute selenite solutions. *Materials (Basel)* 14:286. <https://doi.org/10.3390/ma14020286>
- Osipenko MA, Kharitonov DS, Kasach AA et al (2022) Inhibitive effect of sodium molybdate on corrosion of AZ31 magnesium alloy in chloride solutions. *Electrochim Acta* 414:140175. <https://doi.org/10.1016/j.electacta.2022.140175>
- Kharitonov DS, Zimowska M, Ryl J et al (2021) Aqueous molybdate provides effective corrosion inhibition of WE43 magnesium alloy in sodium chloride solutions. *Corros Sci* 190:109664. <https://doi.org/10.1016/j.corsci.2021.109664>
- Osipenko MA, Kharitonov DS, Makarova IV, Kurilo II (2020) Corrosion behavior of aluminum alloy AD31 in the presence of potassium permanganate in an acidic media. *Prot Met Phys Chem Surfaces* 56:1299–1304. <https://doi.org/10.1134/S2070205120070138>
- Jian SY, Chu YR, Lin CS (2015) Permanganate conversion coating on AZ31 magnesium alloys with enhanced corrosion resistance. *Corros Sci* 93:301–309. <https://doi.org/10.1016/j.corsci.2015.01.040>
- Mosiąłek M, Mordarski G, Nowak P et al (2011) Phosphate-permanganate conversion coatings on the AZ81 magnesium alloy: SEM, EIS and XPS studies. *Surf Coatings Technol* 206:51–62. <https://doi.org/10.1016/j.surfcoat.2011.06.035>
- Song M-S, Deng Q-S, Toh RJ et al (2022) Permanganate, molybdate and vanadate conversion coatings. *Conversion Coatings for Magnesium and its Alloys*. Springer International Publishing, Cham, pp 113–131
- del Olmo R, Mohedano M, Matykina E, Arrabal R (2022) Permanganate loaded Ca-Al-LDH coating for active corrosion protection of 2024–T3 alloy. *Corros Sci* 198:110144. <https://doi.org/10.1016/j.corsci.2022.110144>
- Papavinasam S (2011) Corrosion inhibitors. *Uhlig's Corrosion Handbook*. John Wiley & Sons Inc, Hoboken, NJ, USA, pp 1021–1032
- Baril G, Galicia G, Deslouis C et al (2007) An impedance investigation of the mechanism of pure magnesium corrosion in sodium sulfate solutions. *J Electrochem Soc* 154:C108–C113. <https://doi.org/10.1149/1.2401056>
- King AD, Birbilis N, Scully JR (2014) Accurate electrochemical measurement of magnesium corrosion rates; a combined impedance, mass-loss and hydrogen collection study. *Electrochim Acta* 121:394–406. <https://doi.org/10.1016/j.electacta.2013.12.124>

34. Pawar S, Zhou X, Thompson GE et al (2015) The role of inter-metallics on the corrosion initiation of twin roll cast AZ31 Mg Alloy. *J Electrochem Soc* 162:C442–C448. <https://doi.org/10.1149/2.0291509jes>
35. Eckermann F, Suter T, Uggowitzer PJ et al (2008) The influence of MgSi particle reactivity and dissolution processes on corrosion in Al–Mg–Si alloys. *Electrochim Acta* 54:844–855. <https://doi.org/10.1016/j.electacta.2008.05.078>
36. Osipenko MA, Kharitonov DS, Makarova IV et al (2020) The effect of sealing with potassium permanganate on corrosion resistance of anodized AD31 aluminum alloy. *Prot Met Phys Chem Surfaces* 56:990–997. <https://doi.org/10.1134/S2070205120050214>
37. Dawson P, Hadfield CD, Wilkinson GR (1973) The polarized infra-red and Raman spectra of Mg(OH)<sub>2</sub> and Ca(OH)<sub>2</sub>. *J Phys Chem Solids* 34:1217–1225. [https://doi.org/10.1016/S0022-3697\(73\)80212-4](https://doi.org/10.1016/S0022-3697(73)80212-4)
38. Maltseva A, Shkirskiy V, Lefèvre G, Volovitch P (2019) Effect of pH on Mg(OH)<sub>2</sub> film evolution on corroding Mg by in situ kinetic Raman mapping (KRM). *Corros Sci* 153:272–282. <https://doi.org/10.1016/j.corsci.2019.03.024>
39. Julien CM, Massot M, Poinignon C (2004) Lattice vibrations of manganese oxides: part I. Periodic structures. *Spectrochim Acta - Part A Mol Biomol Spectrosc* 60:689–700. [https://doi.org/10.1016/S1386-1425\(03\)00279-8](https://doi.org/10.1016/S1386-1425(03)00279-8)
40. Cheng S, Yang L, Chen D et al (2014) Phase evolution of an alpha MnO<sub>2</sub>-based electrode for pseudo-capacitors probed by in operando Raman spectroscopy. *Nano Energy* 9:161–167. <https://doi.org/10.1016/j.nanoen.2014.07.008>
41. Sun M, Lan B, Lin T et al (2013) Controlled synthesis of nanostructured manganese oxide: crystalline evolution and catalytic activities. *CrystEngComm* 15:7010. <https://doi.org/10.1039/c3ce40603b>
42. Bernard M, Goff AH, Thi BV et al (1993) Electrochromic reactions in manganese oxides. I. Raman Analysis. *J Electrochem Soc* 140:3065–3070. <https://doi.org/10.1149/1.2220986>
43. Puigdomenech I (2010) Hydra/Medusa chemical equilibrium database and plotting software
44. Song G, Atrens A, John DS et al (1997) The anodic dissolution of magnesium in chloride and sulphate solutions. *Corros Sci* 39:1981–2004. [https://doi.org/10.1016/S0010-938X\(97\)00090-5](https://doi.org/10.1016/S0010-938X(97)00090-5)
45. Song GL, Atrens A (1999) Corrosion mechanisms of magnesium alloys. *Adv Eng Mater* 1:11–33. [https://doi.org/10.1002/\(SICI\)1527-2648\(199909\)1:1%3c11::AID-ADEM11%3e3.0.CO;2-N](https://doi.org/10.1002/(SICI)1527-2648(199909)1:1%3c11::AID-ADEM11%3e3.0.CO;2-N)
46. Song G, Atrens A, Stjohn D et al (1997) The electrochemical corrosion of pure magnesium in 1 N NaCl. *Corros Sci* 39:855–875. [https://doi.org/10.1016/S0010-938X\(96\)00172-2](https://doi.org/10.1016/S0010-938X(96)00172-2)

**Publisher's Note** Springer Nature remains neutral with regard to jurisdictional claims in published maps and institutional affiliations.